CHEMISTRY OF MATERIALS

pubs.acs.org/cm

Article

Unassisted Uranyl Photoreduction and Separation in a Donor–Acceptor Covalent Organic Framework

Yiting Song,[‖] Ao Li,[‖] Pengju Li, Linwei He, Dongyang Xu, Fuqi Wu, Fuwan Zhai, Yutian Wu, Ke Hu,* Shuao Wang,* and Matthew V. Sheridan*

Cite This: *Chem. Mater.* 2022, 34, 2771–2778

Read Online

ACCESS | Metrics & More | Article Recommendations | Supporting Information

ABSTRACT: The donor–acceptor covalent organic framework (COF) **TTT–DTDA** (**TTT** = thieno[3,2-*b*]thiophene-2,5-dicarbaldehyde and **DTDA** = 4,4′,4″-(1,3,5-triazine-2,4,6-triyl)trianiline) was prepared and found to have long-lived excited states (>100 ms) characterized by transient absorption spectroscopy. These excited-state lifetimes were sufficient to perform the direct photoreduction of uranium at ppm concentration levels. The photoreduction of soluble uranyl species to insoluble reduced uranium products is an attractive separation for uranium, typically accomplished with sacrificial reagents and protective gases. In the case of **TTT–DTDA**, illumination in aqueous solutions containing only uranyl ions produced crystalline uranyl peroxide species ($[UO_2(O_2)]$) at the COF that were characterized by powder X-ray diffraction, X-ray photoelectron spectroscopy, and infrared spectroscopy. The maximum absorption capacity of **TTT–DTDA** was found to be 123 mg U/g COF at pH 5 after 10 h of illumination in solutions devoid of sacrificial reagents or protective gases. The **TTT–DTDA** COF was recyclable and maintained high selectivity for uranium in competing ion experiments, which are necessary requirements for a practical uranium extraction strategy based on photochemical uranium reduction.

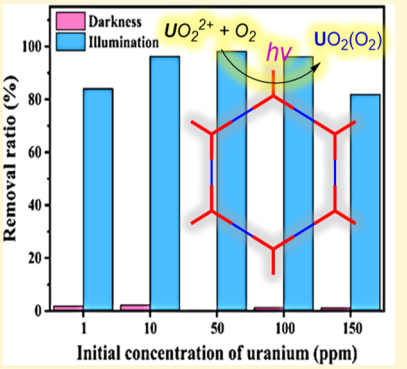

INTRODUCTION

The high energy density and low emissions possible with nuclear energy make it a viable solution, among others, to the global energy problem. Currently, there are over 400 operational nuclear power plants around the world and 60 new plants under construction.[1] The principal fuel and main component of spent fuel in these reactors is uranium.[2] The efficient extraction of uranium from mining sources and seawater (the world's oceans hold up to 4.5 billion tons of uranium)[3] and its separation during radioactive waste water remediation and environmental protection is, therefore, a critical issue concerning nuclear energy as a clean and sustainable energy source. A number of methods have been developed for uranium extraction with many recent examples focusing on the use of highly porous crystalline materials like metal organic frameworks (MOFs)[4] and covalent organic frameworks (COFs).[5] Due to their high porosity, designability, and functionalizability, MOFs and COFs have a high potential for maximum absorption capacities compared to similarly designed polymeric materials. In addition, their synthetic tuneability offers pathways to achieve high selectivity for uranium capture.

A powerful tool in the area of uranium extraction has been to incorporate amidoxime ligands [R(NH$_2$)═N–OH]— which have been found to be highly selective for uranium— into framework and polymeric materials. In particular, amidoxime ligands have been used in materials for successful uranium seawater extraction, overcoming the challenges of low uranium concentration ([U] = 3 ppb), ionic speciation, large number of competing ions, and biofouling that can occur in seawater (Scheme 1 top).[6] In this area, 3D polymer fibers incorporating amidoxime ligands have achieved upward of 17.57 mg U/g material,[7] and MOF and COF materials with amidoxime ligands have achieved 2.68 and 5.12 mg/g absorption capacities in seawater, respectively.[8,9]

To improve selectivity and dramatically increase absorption capacity, other methods have focused on uranium reduction as a strategy. Uranium reduction is a 2e$^-$ process ($U^{VI} + 2e^- \rightarrow U^{IV}$) that produces insoluble uranium precipitates at the material. Advantages of this process are that the material is not saturated by active sites absorption and can produce species with potentially lower solubility than ligand-bound uranium. Till date, materials for uranium reduction have been explored using highly reducing quinones,[10] doped materials with reducing agents such as zero-valent iron,[11] and photocatalysis.[12] Photocatalytic materials are particularly attractive because they are able to use sunlight to produce the reductive

Received: December 23, 2021
Revised: February 6, 2022
Published: March 7, 2022

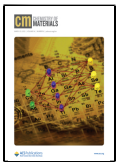

Scheme 1. Uranium Seawater Extraction Strategies: (Top) Polyethylene Polymer with Amidoxime Ligands to Bind Uranium for Seawater Extraction ([U] = 3 ppb); (Bottom) Uranium Photocatalysis to Produce Insoluble Uranium Products

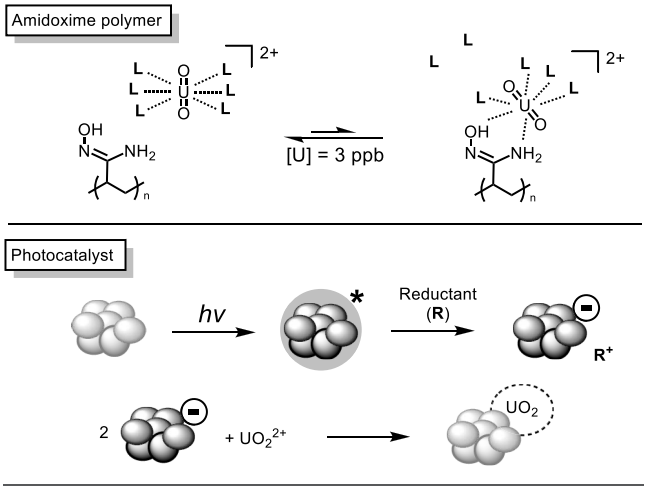

equivalents for uranium reduction from U^{VI} to U^{IV}. This process, however, requires the oxidation of a sacrificial reductant in order to produce charge-neutral insoluble uranium products, Scheme 1 bottom. Promising work in this direction includes a COF with unsubstituted olefin linkages, recently reported to have a uranium absorption capacity up to 2460.8 mg/g using sacrificial reductants and photocatalysis.[13] Other recent materials include highly active donor−acceptor microporous materials with high absorption capacities[14,15] and traditional materials like titanium dioxide (TiO_2)[16] and graphitic carbon nitride[17,18] that have been used with impressive uranium capture abilities (>1 g U absorbed/g material). Nevertheless, all these materials produce reductive equivalents through excited-state oxidation of sacrificial reagents, usually under nitrogen or argon atmospheres, to ensure high photo-efficiencies.[19] On the other hand, an example of uranium reduction under aerobic conditions without sacrificial reagents involved porous electrode materials and an applied electrochemical bias to capture uranium with high selectivity, high faradaic efficiencies for uranium reduction, and impressive absorption capacities.[20,21] An amidoxime-modified carbon felt electrode was reported with an impressive uranium absorption capacity of 1932 mg U/g of electrode material under an applied potential bias.[22]

Here, we present a new photochemical pathway to reduce uranium using a photoactive donor−acceptor COF that works without sacrificial reductants and in the presence of oxygen. To develop a photochemical material for this reaction, the donor−acceptor 2-D COF, **TTT−DTDA**, was prepared, Scheme 2. Donor−acceptor 2-D COFs have emerged as promising photochemical materials due to their excellent charge carrier mobility and impressive excited-state lifetimes, which are attributed to their interlayer π-stacking and unidirectional order.[23] A photophysical study of imine-COF containing fused-bithiophene units similar to the one used here found that the fused-bithiophene linkers provide long-lived excited states that span from an impressive submicroseconds to hundreds of milliseconds.[24] In addition, the **TTT−DTDA** COF does not demonstrate strong dark absorption to uranium or other metals that were tested here, making it ideal to study the uranium photoreduction process. **TTT−DTDA** has also been shown to have high photoactivity to induce free-radical polymerization and could be prepared by the reaction of 4,4′,4″-(1,3,5-triazine-2,4,6-triyl)trianiline (**TTT**), with thieno-[3,2-*b*]thiophene-2,5-dicarbaldehyde (**DTDA**), as described previously.[25]

The reduction of uranium was found to be possible during the long-lived excited state of **TTT−DTDA** characterized by transient absorption (TA) spectroscopy here, producing reduced uranium (UO_2), and propagation of uranyl peroxide was possible by further oxidation of the UO_2 precipitate with solution oxygen: $U^{IV}O_2 + O_2^{2-} \rightarrow U^{VI}O_2(O_2)$. The oxidative equivalents that build up in the COF during the uranium photoreduction process can be removed by solution species or stored in the COF via reactions with the solution vide infra.

Uranium absorption experiments performed with **TTT−DTDA** in pH 2−6 solutions under prolonged UV light illumination with uranium demonstrated markedly increased uranium absorption compared to dark experiments confirmed by inductively coupled plasma atomic emission spectroscopy (ICP−AES). Powder X-ray diffraction (PXRD) was used to confirm the formation of uranyl peroxide, $UO_2(O_2)$, and X-ray photoelectron spectroscopy (XPS) confirmed U(VI) in the material. Based on the uranium removal percent and degree of sulfur oxidation determined by XPS, the faradaic efficiency for **TTT−DTDA** was determined to be 51.3%. TA experiments of **TTT−DTDA** observed long excited-state lifetimes in the COFs (>100 ms). These lifetimes are essential for the successful photoreduction of uranium in dilute solutions such as those found here (1−100 ppm U) and those encountered in radioactive waste water remediation and environmental

Scheme 2. Synthesis of the 2D Donor−Acceptor COF, TTT−DTDA, and Relevant Reactions for the Photoreduction of Uranium

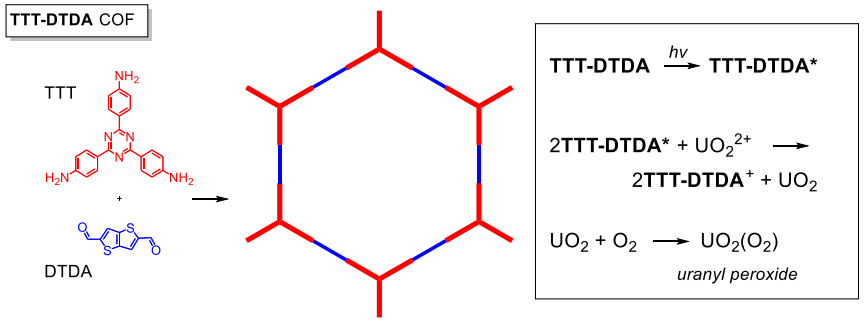

https://doi.org/10.1021/acs.chemmater.1c04407
Chem. Mater. 2022, 34, 2771−2778

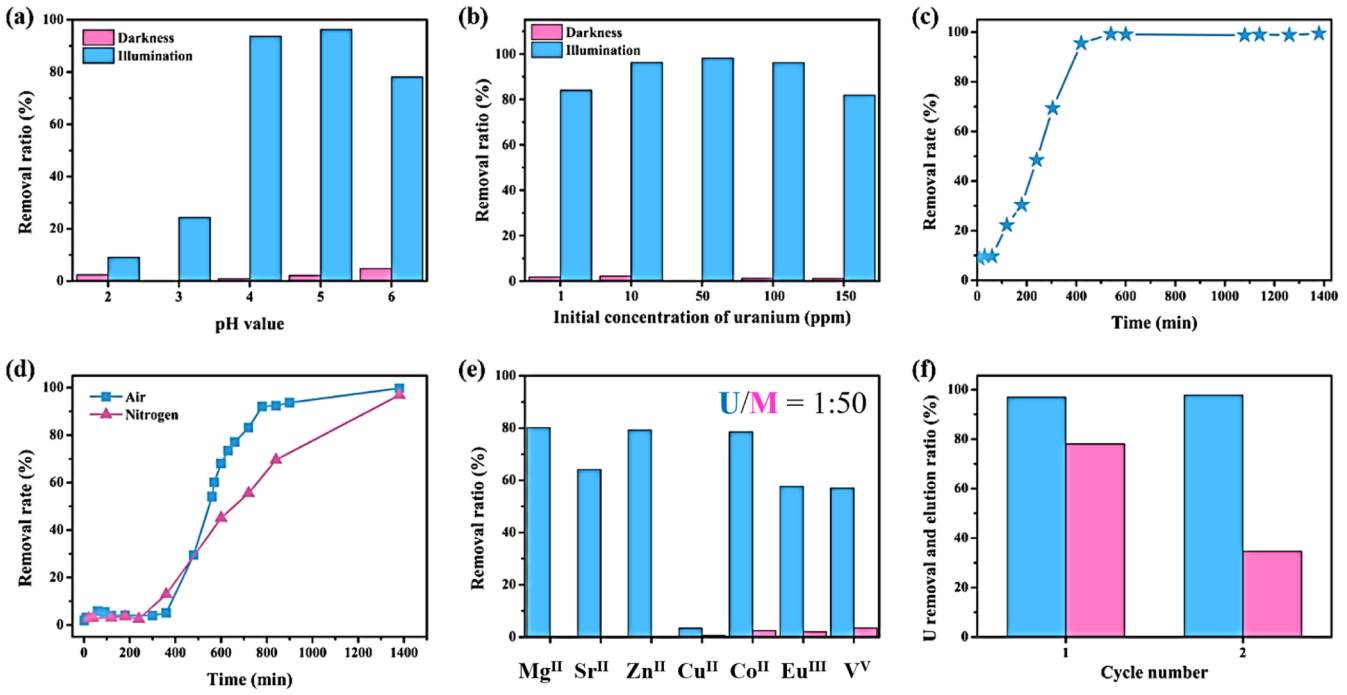

Figure 1. (a) Effect of pH on U absorption for **TTT−DTDA**, [U] ≈ 10 ppm, m/V = 1 g/L, t = 10 h, and T = 300 K; (b) effect of the U concentration for **TTT−DTDA**, pH = 5, m/V = 1 g/L, t = 10 h, and T = 300 K; (c) kinetic data for the photochemical reaction under air condition, [U] ≈ 25 ppm, pH = 5, m/V = 1 g/L; (d) kinetic traces in the presence (gray) and absence (red) of O_2 via purging with nitrogen gas, [U] ≈ 50 ppm, pH = 5, m/V = 1 g/L; and (e) extraction efficiency of U (blue) and other competing ions (red). U/M = 1:50, U = UO_2^{2+}; M = Mg^{II}, Sr^{II}, Zn^{II}, Cu^{II}, Co^{II}, Eu^{III}, and V^{V}, pH = 5, t = 12 h, m/V = 1 g/L; (f) extraction efficiency of U (blue) and elution efficiency using 0.1 M HCl (red) in two cycles, [U] ≈ 100 ppm, pH = 4.0, m/V = 1 g/L, t = 10 h. The experimental data can be found in Supporting Information, Tables S1−S3.

protection separation. Other multi-junction materials have been developed recently for uranium photoreduction, highlighting a necessity for long-lived charge-separated states in uranium photoreduction.[26−28] **TTT−DTDA** removed 94.7% of uranium up to 100 ppm and had a maximum absorption of 123 mg U/g COF at pH 5 after 10 h of illumination ([U] = 150 ppm, **TTT−DTDA** = 1 g/1 L). The material could also be recycled without loss of its photoactivity and maintained its selectivity for uranium in the presence of competing ions.

EXPERIMENTAL SECTION

Materials. **TTT** was purchased from Shanghai Aladdin Biochemical Technology Co., Ltd. **DTDA** was purchased from Shanghai Tensus Biotech Co., Ltd. Mesitylene, dioxane, and acetic acid were purchased from Chinasun Specialty Products Co., Ltd. Metal salts, sodium hydroxide, and nitric acid were purchased from Sigma-Aldrich. Specially, uranyl nitrate, $UO_2(NO_3)_2{\cdot}6H_2O$, purchased from Shenzhen Isotope Industrial International Co., Ltd., was used in all uranium solutions, and given the radioactivity of uranium, weighing and dissolving of uranyl salt were carried out in a dedicated actinide laboratory. All other commercial reagents were used without further purification.

Synthesis. The **TTT−DTDA** COF was prepared, as previously described.[25] Briefly, a solvothermal reaction was carried out between **TTT** (10.6 mg, 0.030 mmol) and **DTDA** (8.8 mg, 0.045 mmol) in the presence of 6 M acetic acid (0.05 mL) and mesitylene/dioxane (0.5 mL) as the solvents. The supernatant was removed, and the precipitate was extracted with supercritical CO_2 (40 °C, 90 bar, 2 h) to yield the COF as an orange powder. The infrared (IR) and PXRD of the COF were in good agreement with reported values.

Characterization Methods. PXRD data were collected on a Bruker D8 Advance diffractometer using Cu Kα radiation at 40 kV, 40 mA power. Fourier transform IR spectra of the samples were characterized using a Thermo Nicolet iS50 spectrometer. XPS spectra were obtained using a Thermo Scientific ESCALAB 250 Xi spectrometer equipped with a monochromatic Al Kα X-ray. Photolysis experiments were carried out in a CEL-LAB200E7 parallel photoreactor using 365 nm light source at 34 V, 3.5 A power (I = 150 mW/cm^2). The thermogravimetric analysis (TGA) measurement was accomplished on a JUPITER STA 449F3 instrument from 30 to 900 °C at a heating rate of 10 °C·min^{-1} under 20 mL·min^{-1} N_2 flow. Scanning electron microscopy (SEM) images were obtained using a field-emission scanning electron microscope (Merlin Compact, Zeiss) at a 10.0 kV acceleration voltage, and all samples were coated with gold to improve the electronic conduction. Energy-dispersive X-ray spectroscopy (EDS) mapping of elements was collected using an FEI Talos F200X4 field-emission transmission electron microscope with an accelerating voltage of 200 kV. Concentrations of uranium were tested on an Agilent 7800 ICP−MS, and concentrations of other metal ions in competing experiments were tested on an iCAP 7000 ICP−AES using the standard curve method.

Uranium Absorption Experiments. An amount of the **TTT−DTDA** COF sample in the range of 6−7 mg was placed in a 20 mL glass bottle with a lid, and then, the corresponding amount of uranyl nitrate solution with adjusted pH value was added, keeping the solid−liquid ratio equal to 1:1 g/L. With stirring, the container was placed under illumination (λ = 365 nm) or covered with aluminum foil to ensure a dark environment. The effect of the pH value for UO_2^{2+} extraction was carried out in the pH range of 2−6. In general, 10 mg of **TTT−DTDA** was added to 10 mL of 10 ppm UO_2^{2+} solution with different pH values. After being stirred for 10 h, the solution was separated using a 0.22 μm nylon membrane filter for ICP analysis. The data are reported as an average of two to three samples. The effect of competing ions was studied by adding different concentrations of $Mg(NO_3)_2$, $Sr(NO_3)_2$, $Zn(NO_3)_2{\cdot}6H_2O$, $Cu(NO_3)_2{\cdot}6H_2O$, $Co(NO_3)_2{\cdot}6H_2O$, $Eu(NO_3)_3{\cdot}6H_2O$, and $NaVO_3$ into 10 ppm UO_2^{2+} solution, respectively. After being stirred for 12 h, the

https://doi.org/10.1021/acs.chemmater.1c04407
Chem. Mater. 2022, 34, 2771−2778

solution was separated using a 0.22 μm nylon membrane filter for ICP analysis.

Kinetics. Experiments were carried out at pH 5 with a solid−liquid ratio of 1 g material per liter solution. In each sample, 150 mg of material was added to 150 mL of 25 ppm UO_2^{2+} solution. To determine the U concentration, 1 mL of the solution was taken out after stirring for 10 min, 30 min, 1 h, 2 h, 3 h, 4 h, 5 h, 7 h, 9 h, 10 h, and 18 h, respectively. The samples were separated using a 0.22 μm nylon membrane filter for ICP analysis. Recycle experiments were first tested with 10 mg of **TTT−DTDA** added to 10 mL of 100 ppm UO_2^{2+} solution at pH 5. After 12 h of stirring, **TTT−DTDA** was separated from the solution by filtration. The UO_2^{2+}-loaded **TTT−DTDA** sample was dried naturally in air, and the solution was measured by ICP to get the concentration in order to determine the extraction efficiency of the first use of **TTT−DTDA**. Next, the UO_2^{2+}-loaded sample underwent through a desorption process in 10 mL of 0.1 M HCl, 2 M Na_2CO_3, or 0.5 M NaOH with the contact time of 2 h. The UO_2^{2+} concentration for the resulted desorption solution was determined, and the desorption efficiency was obtained for the first use of **TTT−DTDA**. The separated **TTT−DTDA** was dried naturally in air and retested for uranium removal, and desorption was re-evaluated under identical conditions.

TA Spectroscopy. Nanosecond TA spectra were acquired on a TSP-2000 (Unisoku) laser flash photolysis system. Briefly, a Q-switched frequency-tripled pulsed Nd:YAG laser (Quantel Q-Smart 450, 10 Hz) was employed to generate 355 nm laser pulses (5−8 nm full width at half-maximum, 10 mJ/cm^2 per pulse). A 75 W xenon arc lamp with elliptical reflection served as the probe beam that was focused onto the center of the 10 mm cuvette with a combination of convex lenses. The probe beam was aligned orthogonally to the excitation laser beam and was passed into an f/300 mm monochromator (Acton, Princeton Instrument) that coupled with an R2949 photomultiplier tube (Hamamatsu) to achieve the signal detection. TA data at each wavelength were acquired on a computer interfaced digital oscilloscope (LeCroy 4024, 12 bit, 200 MHz) with typical 50 laser pulse averages. TA data on longer time scales were acquired with a series of system built-in resistors to optimize the signal-to-noise ratio. Data were processed in Origin 9 and fit with least-squares error minimization using the Levenberg−Marquardt iteration method.

RESULTS AND DISCUSSION

Extraction Performance. The initial tests of the COF (1 g material/1 L solution) in uranium absorption experiments were performed under ambient conditions at pH 2, 3, 4, 5, and 6 ([U] ∼ 10 ppm) with 10 h of illumination, Figure 1a. The pH of the solution was controlled using dilute NaOH or HNO_3 solution. The extraction performance under light illumination increased with increasing pH as has been described in other reports and is consistent with the deprotonation of uranium species and formation of charged-neutral insoluble products.[9] At more basic pHs, the solubility of uranium increases, dependent on the anions present in solution forming more soluble negatively charged complexes, such as uranyl tris-carbonate, $[UO_2(CO_3)_3]^{4-}$.[29] Under the best conditions, pH 5, uranium removal reached 96.3% in the light and in dark experiments. <5% of uranium removal was observed in all experiments. The effect of the concentration of uranium is shown in Figure 1b. After 10 h of illumination, the **TTT−DTDA** COF could absorb up to 98.2% of uranium at 50 ppm and 81.9% at [U] = 150 ppm for a maximum absorption capacity under these conditions of 123 mg U/1 g **TTT−DTDA**.

The kinetics of U absorption were evaluated at pH 5 and [U] = 25 ppm. The results are shown in Figure 1c, showing a gradual increase in U absorption over time after an initial phase with zero absorption. The onset period was dependent on the concentration of uranium with higher concentration of uranium producing longer initial incubation periods prior to uranium absorption being observed (Figure S1). Control experiments with the starting material **TTT** and **DTDA** showed low uranium removal percents and no photochemically induced activity (Figures S2 and S3). A similar effect was observed with competing ions described later where the presence of additional ions reduced uranium absorption. This incubation period is attributed to the formation of U^{IV} precipitates followed by further absorption of uranyl ions, uranium reduction, and crystal growth.[22,30] This mechanism is consistent with the results for electrochemical formation of uranyl peroxide and characterization of the material described later.[22] Specifically, significant material degradation is not observed from unproductive oxygen reduction, and, in TA spectroscopy, the excited-state decay lifetimes are not significantly perturbed by the presence of oxygen.

Next, the uranium uptake kinetics were studied in a solution, which continuously bubbled with nitrogen gas, Figure 1d. A much slower rate of uranium removal at the material was observed, whereas the initial incubation period remained largely unchanged. It is proposed that advantageous oxygen is responsible for the uranium absorption observed in the nitrogen gas experiments, which is enabled by the ppm level of uranium being removed and the long time period of the experiment. In this experiment, the chemical reaction of oxygen is rate limiting, following formation of U^{IV} seeds. In competing ions experiments described next, none of the competing ions were absorbed at the material in any of the experiments. This suggests that the formation of new ligand active sites does not occur upon illumination of the COF during the incubation period or any period of the experiment, and that, the process is strictly due to the photochemical properties of the material, which allows for photoreduction and uranium absorption.

The selectivity of U absorption was tested against five different ions for competitive adsorption with uranium in the **TTT−DTDA** photochemical experiments and their effect on the uranium absorption performance. The ions Mg^{2+}, Sr^{2+}, Zn^{2+}, Cu^{2+}, Co^{2+}, Eu^{3+}, and VO_3^- were selected based on their ionic charge, speciation, or relevant redox activity and tested at a 50:1 ratio to uranium. In the case of Mg^{2+}, Sr^{2+}, Zn^{2+}, Co^{2+}, Eu^{3+}, and VO_2^+, a decrease in uranium absorption capacity was observed after 12 h of illumination (Figure 1e). In the presence of Cu, neither metal showed uptake at the material and possibly due to the redox $Cu^{II/I}$ that is accessible at similar potentials as the $U^{VI/V}$ redox couple or excited-state quenching by copper species.[31,32] To ensure the durability of the material even after extensive photolysis in aqueous solutions in the presence of oxygen, recycling experiments were performed. Following a uranium experiment, the material was washed with 0.1 M hydrochloric acid, 2 M carbonate, or basic sodium hydroxide (0.1 M) solutions and retested under the same conditions. In all cases, the material could be recycled with the acid wash being the most effective, and the material exhibited no loss in the performance in subsequent photochemical experiments (Figures S4 and 1f). The material is still subject to continued oxidative stress from the experiments and will need to be regenerated eventually. However, the impressive photochemical performance under such harsh conditions is promising for the practical use of COFs in this application.

Material Characterization. Following photochemical experiments at pH 5, [U] = 50 ppm, **TTT−DTDA** was

https://doi.org/10.1021/acs.chemmater.1c04407
Chem. Mater. 2022, 34, 2771−2778

characterized by PXRD, IR, and XPS. The PXRD shows a diminished signal for the COF; however, the characteristic signals appear at 16.9, 20.2, 23.4, 25.0, and 27.3 for $(UO_2)O_2$, as seen in previous peroxide-mediated electrochemical uranium depositions and other photochemical reductions (Figure 2a).[12,33] The loss of crystallinity in the COF occurs during the photolysis and is attributed to a degree of exfoliation due to photochemical intermediates such as protons being introduced during the experiment.[34] A color change associated with protonation of the COF was observed in all experiments, which could be regenerated with base (Figure S5). In the IR, many of the initial **TTT−DTDA** peaks remain after uranium experiments with new peaks for $(UO_2)O_2$ appearing at 931 and 1434 cm^{-1} (Figure 2b).[35] The XPS of the material after photolysis and uranyl peroxide formation shows only U(VI) peaks (Figure 2c), similar to the electrochemical formation of uranyl peroxide, which was found to be a highly selective and efficient process to produce uranyl peroxide based on the electrolysis and Coulombic efficiency.[22] The XPS in the area of N 1s and S 2p shows not only diminished signals likely associated with a U blocking layer but also an increase in peaks for higher oxidation products such as the 168 eV peak for S 2p (Figures S6−S8), which is indicative of an S,S-oxide, and a shift in the N 1s region, which can either be associated with protonation or amine oxidation and amide formation (−C═N− → −C(O)−NH−).[36,37]

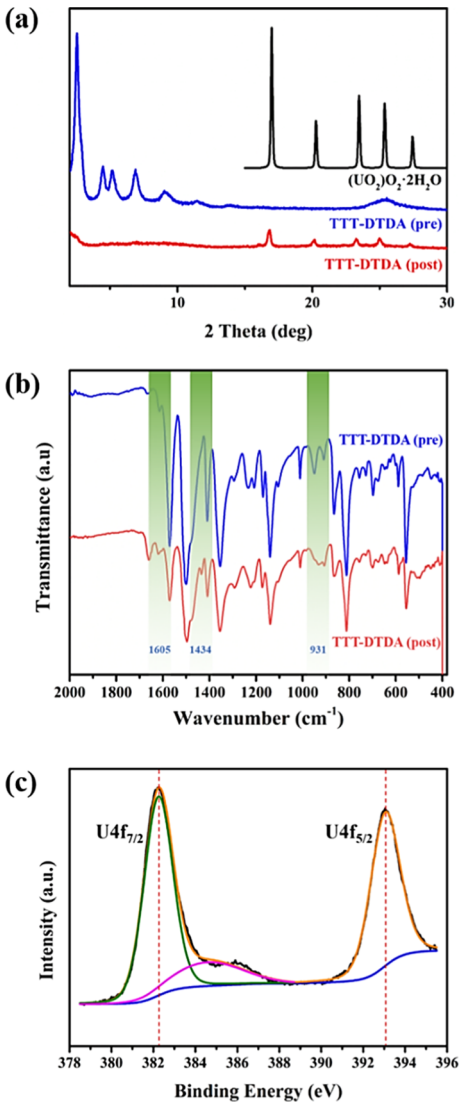

Figure 2. (a) PXRD of **TTT−DTDA** before and after the photochemical experiments [inset: $(UO_2)O_2$ reference]; (b) IR of the material before and after highlighting the appearance of new peaks; and (c) XPS of the samples after photolysis in the U 4f region.

Additionally, in the IR region, a new signal appears at 1605 cm^{-1}, which may be attributed to one of the decomposition products. Evidence for the protonation of the imine is consistent with the color change observed and IR for recently described protonated imine-COFs (Figures S5 and S8).[25,38,39] The solid-state ^{13}C NMR of samples before and after photochemical experiments do not show discernible downfield peaks suggestive of carbonyl species or a clear signal for protonation making the reaction occurring along the imine bond difficult to assign (Figure S9).[38] Nevertheless, the COF remains principally intact based on peak changes in XPS and solid-state ^{13}C NMR, suggesting that the photoconversion efficiency of uranium at the COF is relatively high, and excessive decomposition does not occur. Based on the four-electron oxidation of sulfur to $-SO_2-$ and a two-electron reduction of uranium, an upper limit for the maximum photoconversion efficiency of 51.9% was obtained (see the Supporting Information for details). Finally, material characterization of **TTT−DTDA** with SEM, TEM, EDS, and TGA was performed and showed a well-dispersed distribution of uranium in the samples following photochemical experiments (Figures S10−S13).

Photophysics. The photoreactivity of **TTT−DTDA** toward uranium reduction at the ppm level is a remarkable achievement. Most reported COF materials only showed excited-state lifetimes on the subnanosecond time scale.[40] Efficient photoreduction with photosensitizer excited-state lifetimes at the ultrafast time scale is rarely observed due to the diffusion-limited bimolecular reaction. This problem is highlighted by the frequent use of sacrificial reagents and protective gases to perform uranium photoreactions at framework materials.[19] Nanosecond TA measurements were carried out to further understand the **TTT−DTDA** photoreactivity. As shown in Figure 3a, there is the full TA spectra for **TTT−DTDA** dispersed in acetonitrile under ambient air. A photoinduced absorption peaked at 390 nm was observed right after the nanosecond laser pulse at 30 ns delay time. The absorption profile also has an absorption shoulder at around 450 nm and a broad absorption tail that extends into the near IR region. In the submicrosecond time domain, the excited state of **TTT−DTDA** follows a single exponential kinetic decay with the characteristic decay time constant of 0.25 μs, as shown in Figure 3b inset. The TA spectra then reach a kinetic plateau from microseconds to submilliseconds until decaying again back to the baseline with the characteristic single exponential decay time constant of 94 ms, Figure 3b. Note that after entering the microsecond time domain, the photoinduced absorption spectra seem to lose the absorption shoulder at around 450 nm and the broad absorption tail in the red region.

The remarkably long-lived excited state of **TTT−DTDA**, that spans from nanoseconds to almost a second, could be a triplet exciton, but a prior study on the excited-state dynamics of COFs based on a similar fused-bithiophene unit disputed this possibility and suggested the charge-separated state.[24] The attribution to a long-lived charge-separated state was supported

https://doi.org/10.1021/acs.chemmater.1c04407
Chem. Mater. 2022, 34, 2771−2778

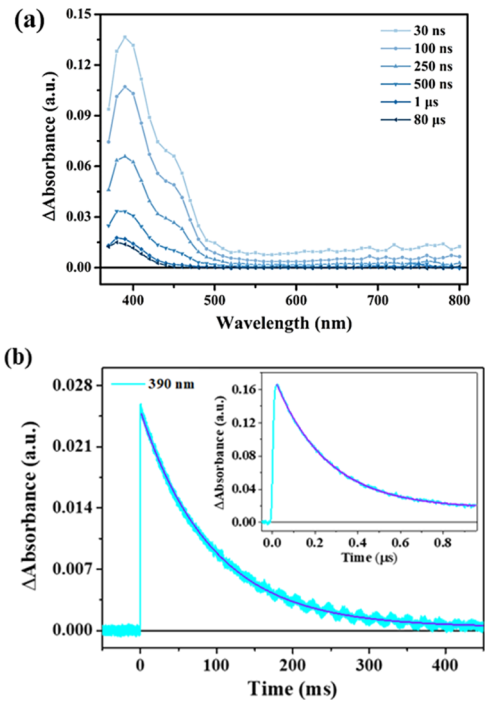

Figure 3. (a) Absorption difference spectra measured after 355 nm pulsed laser excitation at indicated delay times for **TTT−DTDA** dispersed in acetonitrile under ambient air. Absorption changes as a function of time on the scale of submicrosecond (inset) and subsecond monitored at 390 nm after 355 nm pulsed laser excitation (laser fluence of 10 mJ/cm^2). Overlaid in blue is the single-exponential fit to the kinetic data.

by a weak and broad absorption in the red and near IR regions, which is also observed in our nanosecond TA spectra. Therefore, we attribute the observed photoinduced long-lived absorption to a charge-separated state.

The charge-separated state returns to the ground state through possible trap-assisted recombination as was previously assigned.[41] The multiexponential kinetics that span over orders of magnitude are reminiscent of the widely studied charge recombination at the molecular sensitizer-metal oxide interfaces that also showed microsecond to millisecond long lifetimes.[42] The intriguing loss of the absorption shoulder at 450 nm and the broad weakly absorbing feature from microseconds to subseconds is attributed to a possible structural change within the COF, which could be the cause of the subtle absorption change from the charge-separated state and the breakdown of the continuous kinetic decay (Figure S14). If this hypothesis is correct, then future design of the long-lived COF could be based on this point. This kinetic feature will be exploited in future studies.

CONCLUSIONS

The 2D donor−acceptor COF, **TTT−DTDA**, was studied for unassisted uranium capture under aerobic conditions and UV light illumination. The **TTT−DTDA** COF was found to effectively remove uranium from solution via uranium photoreduction and follow-up reactions with oxygen to form crystalline uranyl peroxide precipitates (the maximum absorption of 123 mg U/g COF at pH 5). Uranium absorption was confirmed by ICP−AES, PXRD, XPS, and IR spectroscopy. The promising photochemical properties of **TTT−DTDA** were established by TA spectroscopy. The remarkably long-lived excited state associated with the fused-biothiophene linker was characterized (>100 ms) and allows for the bimolecular reaction between the material and uranyl ions at ppm concentrations to occur during the excited-state window. Using photoactive COFs to produce insoluble uranyl peroxide without sacrificial reagents in the presence of oxygen is a highly promising strategy to overcome the limits associated with traditional materials based on ligand absorption. In this regard, the low concentration of uranium in environments like seawater disfavors equilibrium absorption at the material, and, in contrast, to the solubility conditions for uranyl peroxide. Uranyl peroxide produced by uranium reduction is dependent on the peroxide concentration and forms large peroxide clusters at elevated pH, which are promising features to solve separation issues at ppb concentrations.[43] The current results with **TTT−DTDA** in aqueous solutions without sacrificial reagents and protective gases for uranium extraction are promising for practical use in radioactive waste water remediation and environmental protection.

ASSOCIATED CONTENT

Supporting Information

The Supporting Information is available free of charge at https://pubs.acs.org/doi/10.1021/acs.chemmater.1c04407.

Additional methods, kinetic and absorption data, including photographs of experiments, and XPS, ^{13}C NMR, SEM, TEM, EDS, TGA, and TA spectra of the material (PDF)

AUTHOR INFORMATION

Corresponding Authors

Ke Hu − *Department of Chemistry, Fudan University, Shanghai 200433, China;* orcid.org/0000-0002-0240-7192; Email: khu@fudan.edu.cn

Shuao Wang − *State Key Laboratory of Radiation Medicine and Protection, School for Radiological and Interdisciplinary Sciences (RAD-X) and Collaborative Innovation Center of Radiation Medicine of Jiangsu Higher Education Institutions, Soochow University, Suzhou 215123, China;* orcid.org/0000-0002-1526-1102; Email: shuaowang@suda.edu.cn

Matthew V. Sheridan − *State Key Laboratory of Radiation Medicine and Protection, School for Radiological and Interdisciplinary Sciences (RAD-X) and Collaborative Innovation Center of Radiation Medicine of Jiangsu Higher Education Institutions, Soochow University, Suzhou 215123, China;* orcid.org/0000-0001-9950-154X; Email: matt1@suda.edu.cn

Authors

Yiting Song − *State Key Laboratory of Radiation Medicine and Protection, School for Radiological and Interdisciplinary Sciences (RAD-X) and Collaborative Innovation Center of Radiation Medicine of Jiangsu Higher Education Institutions, Soochow University, Suzhou 215123, China*

Ao Li − *State Key Laboratory of Radiation Medicine and Protection, School for Radiological and Interdisciplinary Sciences (RAD-X) and Collaborative Innovation Center of Radiation Medicine of Jiangsu Higher Education Institutions, Soochow University, Suzhou 215123, China*

Pengju Li − *Department of Chemistry, Fudan University, Shanghai 200433, China*

https://doi.org/10.1021/acs.chemmater.1c04407
Chem. Mater. 2022, 34, 2771−2778

Linwei He − *State Key Laboratory of Radiation Medicine and Protection, School for Radiological and Interdisciplinary Sciences (RAD-X) and Collaborative Innovation Center of Radiation Medicine of Jiangsu Higher Education Institutions, Soochow University, Suzhou 215123, China*

Dongyang Xu − *School of Resources & Environment and Safety Engineering, University of South China, Hengyang, Hunan 421001, China*

Fuqi Wu − *State Key Laboratory of Radiation Medicine and Protection, School for Radiological and Interdisciplinary Sciences (RAD-X) and Collaborative Innovation Center of Radiation Medicine of Jiangsu Higher Education Institutions, Soochow University, Suzhou 215123, China*

Fuwan Zhai − *State Key Laboratory of Radiation Medicine and Protection, School for Radiological and Interdisciplinary Sciences (RAD-X) and Collaborative Innovation Center of Radiation Medicine of Jiangsu Higher Education Institutions, Soochow University, Suzhou 215123, China*

Yutian Wu − *State Key Laboratory of Radiation Medicine and Protection, School for Radiological and Interdisciplinary Sciences (RAD-X) and Collaborative Innovation Center of Radiation Medicine of Jiangsu Higher Education Institutions, Soochow University, Suzhou 215123, China*

Complete contact information is available at: https://pubs.acs.org/10.1021/acs.chemmater.1c04407

Author Contributions

[‖]Y.S. and A.L. contributed equally to this paper.

Notes

The authors declare no competing financial interest.

■ ACKNOWLEDGMENTS

M.V.S. acknowledges startup funding from the Soochow University. Y.S., A.L., D.X., Y.W., and M.V.S. work was supported by the National Natural Science Foundation of China (22050410278). L.H., F.W., F.Z., and S.W. acknowledge support from the National Natural Science Foundation (21825601 and 21790374). P.L. and K.H. would like to thank the financial support from the National Natural Science Foundation of China (21872037).

■ REFERENCES

(1) Mathew, M. D. Nuclear energy: A pathway towards mitigation of global warming. *Prog. Nucl. Energy* **2022**, *143*, 104080.

(2) Ewing, R. C. Long-term storage of spent nuclear fuel. *Nat. Mater.* **2015**, *14*, 252−257.

(3) Maher, K.; Bargar, J. R.; Brown, G. E. Environmental Speciation of Actinides. *Inorg. Chem.* **2013**, *52*, 3510−3532.

(4) Yang, W.; Pan, Q.; Song, S.; Zhang, H. Metal−organic framework-based materials for the recovery of uranium from aqueous solutions. *Inorg. Chem. Front.* **2019**, *6*, 1924−1937.

(5) Cheng, G.; Zhang, A.; Zhao, Z.; Chai, Z.; Hu, B.; Han, B.; Ai, Y.; Wang, X. Extremely stable amidoxime functionalized covalent organic frameworks for uranium extraction from seawater with high efficiency and selectivity. *Sci. Bull.* **2021**, *66*, 1994−2001.

(6) Yuan, Y.; Yu, Q.; Cao, M.; Feng, L.; Feng, S.; Liu, T.; Feng, T.; Yan, B.; Guo, Z.; Wang, N. Selective extraction of uranium from seawater with biofouling-resistant polymeric peptide. *Nat. Sustain.* **2021**, *4*, 708−714.

(7) Xu, X.; Xu, L.; Ao, J.; Liang, Y.; Li, C.; Wang, Y.; Huang, C.; Ye, F.; Li, Q.; Guo, X.; et al. Ultrahigh and economical uranium extraction from seawater via interconnected open-pore architecture poly-(amidoxime) fiber. *J. Mater. Chem. A* **2020**, *8*, 22032−22044.

(8) Chen, L.; Bai, Z.; Zhu, L.; Zhang, L.; Cai, Y.; Li, Y.; Liu, W.; Wang, Y.; Chen, L.; Diwu, J.; et al. Ultrafast and Efficient Extraction of Uranium from Seawater Using an Amidoxime Appended Metal−Organic Framework. *ACS Appl. Mater. Interfaces* **2017**, *9*, 32446−32451.

(9) Abney, C. W.; Mayes, R. T.; Saito, T.; Dai, S. Materials for the Recovery of Uranium from Seawater. *Chem. Rev.* **2017**, *117*, 13935−14013.

(10) Li, Y.; Guo, X.; Li, X.; Zhang, M.; Jia, Z.; Deng, Y.; Tian, Y.; Li, S.; Ma, L. Redox-Active Two-Dimensional Covalent Organic Frameworks (COFs) for Selective Reductive Separation of Valence-Variable, Redox-Sensitive and Long-Lived Radionuclides. *Angew. Chem., Int. Ed.* **2020**, *59*, 4168−4175. accessed 2021/08/16

(11) Xu, L.; Zhang, D.; Ma, F.; Zhang, J.; Khayambashi, A.; Cai, Y.; Chen, L.; Xiao, C.; Wang, S. Nano-MOF+ Technique for Efficient Uranyl Remediation. *ACS Appl. Mater. Interfaces* **2019**, *11*, 21619−21626.

(12) Li, H.; Zhai, F.; Gui, D.; Wang, X.; Wu, C.; Zhang, D.; Dai, X.; Deng, H.; Su, X.; Diwu, J.; et al. Powerful uranium extraction strategy with combined ligand complexation and photocatalytic reduction by postsynthetically modified photoactive metal-organic frameworks. *Appl. Catal., B* **2019**, *254*, 47−54.

(13) Cui, W.-R.; Zhang, C.-R.; Xu, R.-H.; Chen, X.-R.; Jiang, W.; Li, Y.-J.; Liang, R.-P.; Zhang, L.; Qiu, J.-D. Rational design of covalent organic frameworks as a groundbreaking uranium capture platform through three synergistic mechanisms. *Appl. Catal., B* **2021**, *294*, 120250.

(14) Yu, F.; Zhu, Z.; Wang, S.; Wang, J.; Xu, Z.; Song, F.; Dong, Z.; Zhang, Z. Novel donor-acceptor-acceptor ternary conjugated microporous polymers with boosting forward charge separation and suppressing backward charge recombination for photocatalytic reduction of uranium (VI). *Appl. Catal., B* **2022**, *301*, 120819.

(15) Yu, F.; Zhu, Z.; Wang, S.; Peng, Y.; Xu, Z.; Tao, Y.; Xiong, J.; Fan, Q.; Luo, F. Tunable perylene-based donor-acceptor conjugated microporous polymer to significantly enhance photocatalytic uranium extraction from seawater. *Chem. Eng. J.* **2021**, *412*, 127558.

(16) Li, P.; Wang, J.; Wang, Y.; Liang, J.; He, B.; Pan, D.; Fan, Q.; Wang, X. Photoconversion of U(VI) by TiO_2: An efficient strategy for seawater uranium extraction. *Chem. Eng. J.* **2019**, *365*, 231−241.

(17) Liu, S.; Wang, Z.; Lu, Y.; Li, H.; Chen, X.; Wei, G.; Wu, T.; Maguire, D.-J.; Ye, G.; Chen, J. Sunlight-induced uranium extraction with triazine-based carbon nitride as both photocatalyst and adsorbent. *Appl. Catal., B* **2021**, *282*, 119523.

(18) Wang, J.; Wang, Y.; Wang, W.; Ding, Z.; Geng, R.; Li, P.; Pan, D.; Liang, J.; Qin, H.; Fan, Q. Tunable mesoporous g-C3N4 nanosheets as a metal-free catalyst for enhanced visible-light-driven photocatalytic reduction of U(VI). *Chem. Eng. J.* **2020**, *383*, 123193.

(19) Li, P.; Wang, J.; Wang, Y.; Liang, J.; Pan, D.; Qiang, S.; Fan, Q. An overview and recent progress in the heterogeneous photocatalytic reduction of U(VI). *J. Photochem. Photobiol., C* **2019**, *41*, 100320.

(20) Zhang, P.; Wang, L.; Huang, Z.; Yu, J.; Li, Z.; Deng, H.; Yin, T.; Yuan, L.; Gibson, J. K.; Mei, L.; et al. Aryl Diazonium-Assisted Amidoximation of MXene for Boosting Water Stability and Uranyl Sequestration via Electrochemical Sorption. *ACS Appl. Mater. Interfaces* **2020**, *12*, 15579−15587.

(21) Wang, L.; Zhao, R.; Gu, Z. j.; Zhao, Y. l.; Chai, Z. f.; Shi, W. q. Growth of Uranyl Hydroxide Nanowires and Nanotubes by the Electrodeposition Method and Their Transformation to One-Dimensional U3O8 Nanostructures. *Eur. J. Inorg. Chem.* **2014**, *2014*, 1158−1164. accessed 2021/08/16

(22) Liu, C.; Hsu, P.-C.; Xie, J.; Zhao, J.; Wu, T.; Wang, H.; Liu, W.; Zhang, J.; Chu, S.; Cui, Y. A half-wave rectified alternating current electrochemical method for uranium extraction from seawater. *Nat. Energy* **2017**, *2*, 17007.

(23) Yang, S.; Hu, W.; Zhang, X.; He, P.; Pattengale, B.; Liu, C.; Cendejas, M.; Hermans, I.; Zhang, X.; Zhang, J.; et al. 2D Covalent Organic Frameworks as Intrinsic Photocatalysts for Visible Light-Driven CO2 Reduction. *J. Am. Chem. Soc.* **2018**, *140*, 14614−14618.

(24) Jakowetz, A. C.; Hinrichsen, T. F.; Ascherl, L.; Sick, T.; Calik, M.; Auras, F.; Medina, D. D.; Friend, R. H.; Rao, A.; Bein, T. Excited-State Dynamics in Fully Conjugated 2D Covalent Organic Frameworks. *J. Am. Chem. Soc.* **2019**, *141*, 11565−11571.
(25) Pachfule, P.; Acharjya, A.; Roeser, J.; Sivasankaran, R. P.; Ye, M.-Y.; Brückner, A.; Schmidt, J.; Thomas, A. Donor−acceptor covalent organic frameworks for visible light induced free radical polymerization. *Chem. Sci.* **2019**, *10*, 8316−8322.
(26) Li, Z.; Zhang, Z.; Dong, Z.; Yu, F.; Ma, M.; Wang, Y.; Wang, Y.; Liu, Y.; Liu, J.; Cao, X.; et al. Solar light-responsive CdS/UiO-66-NH2 for ultrafast uranium reduction from uranium-containing mine wastewater without external sacrificial agents. *Sep. Purif. Technol.* **2022**, *283*, 120195.
(27) Liang, P.; Yuan, L.; Du, K.; Wang, L.; Li, Z.; Deng, H.; Wang, X.; Luo, S.-Z.; Shi, W. Photocatalytic reduction of uranium(VI) under visible light with 2D/1D Ti3C2/CdS. *Chem. Eng. J.* **2021**, *420*, 129831.
(28) Zhang, Y.; Zhu, M.; Zhang, S.; Cai, Y.; Lv, Z.; Fang, M.; Tan, X.; Wang, X. Highly efficient removal of U(VI) by the photoreduction of SnO2/CdCO3/CdS nanocomposite under visible light irradiation. *Appl. Catal., B* **2020**, *279*, 119390.
(29) Mühr-Ebert, E. L.; Wagner, F.; Walther, C. Speciation of uranium: Compilation of a thermodynamic database and its experimental evaluation using different analytical techniques. *Appl. Geochem.* **2019**, *100*, 213−222.
(30) Kubatko, K.-A. H.; Helean, K. B.; Navrotsky, A.; Burns, P. C. Stability of Peroxide-Containing Uranyl Minerals. *Science* **2003**, *302*, 1191−1193. accessed 2021/10/25
(31) Palmer, C. E. A.; McMillin, D. R.; Kirmaier, C.; Holten, D. Flash photolysis and quenching studies of copper(I) systems in the presence of Lewis bases: inorganic exciplexes? *Inorg. Chem.* **1987**, *26*, 3167−3170.
(32) Zhang, Q.; Wilson, P.; Li, Z.; McHale, R.; Godfrey, J.; Anastasaki, A.; Waldron, C.; Haddleton, D. M. Aqueous Copper-Mediated Living Polymerization: Exploiting Rapid Disproportionation of CuBr with Me6TREN. *J. Am. Chem. Soc.* **2013**, *135*, 7355−7363.
(33) Li, Z.; Zhang, Z.; Dong, Z.; Wu, Y.; Zhu, X.; Cheng, Z.; Liu, Y.; Wang, Y.; Zheng, Z.; Cao, X.; et al. CuS/TiO_2 nanotube arrays heterojunction for the photoreduction of uranium (VI). *J. Solid State Chem.* **2021**, *303*, 122499.
(34) Burke, D. W.; Sun, C.; Castano, I.; Flanders, N. C.; Evans, A. M.; Vitaku, E.; McLeod, D. C.; Lambeth, R. H.; Chen, L. X.; Gianneschi, N. C.; et al. Acid Exfoliation of Imine-linked Covalent Organic Frameworks Enables Solution Processing into Crystalline Thin Films. *Angew. Chem., Int. Ed.* **2020**, *59*, 5165−5171. accessed 2021/08/16
(35) Li, Z. D.; Zhang, H. Q.; Xiong, X. H.; Luo, F. U(VI) adsorption onto covalent organic frameworks-TpPa-1. *J. Solid State Chem.* **2019**, *277*, 484−492.
(36) Jiang, T.; Malone, W.; Tong, Y.; Dragoe, D.; Bendounan, A.; Kara, A.; Esaulov, V. A. Thiophene Derivatives on Gold and Molecular Dissociation Processes. *J. Phys. Chem. C* **2017**, *121*, 27923−27935.
(37) Kehrer, M.; Duchoslav, J.; Hinterreiter, A.; Cobet, M.; Mehic, A.; Stehrer, T.; Stifter, D. XPS investigation on the reactivity of surface imine groups with TFAA. *Plasma Processes Polym.* **2019**, *16*, 1800160. accessed 2021/12/22
(38) Yang, J.; Acharjya, A.; Ye, M. Y.; Rabeah, J.; Li, S.; Kochovski, Z.; Youk, S.; Roeser, J.; Grüneberg, J.; Penschke, C.; et al. Protonated Imine-Linked Covalent Organic Frameworks for Photocatalytic Hydrogen Evolution. *Angew. Chem., Int. Ed.* **2021**, *60*, 19797−19803. accessed 2021/12/21
(39) Ascherl, L.; Evans, E. W.; Gorman, J.; Orsborne, S.; Bessinger, D.; Bein, T.; Friend, R. H.; Auras, F. Perylene-Based Covalent Organic Frameworks for Acid Vapor Sensing. *J. Am. Chem. Soc.* **2019**, *141*, 15693−15699.
(40) Keller, N.; Bein, T. Optoelectronic processes in covalent organic frameworks. *Chem. Soc. Rev.* **2021**, *50*, 1813−1845.
(41) Hu, K.; Sampaio, R. N.; Schneider, J.; Troian-Gautier, L.; Meyer, G. J. Perspectives on Dye Sensitization of Nanocrystalline Mesoporous Thin Films. *J. Am. Chem. Soc.* **2020**, *142*, 16099−16116.
(42) Ashford, D. L.; Gish, M. K.; Vannucci, A. K.; Brennaman, M. K.; Templeton, J. L.; Papanikolas, J. M.; Meyer, T. J. Molecular Chromophore−Catalyst Assemblies for Solar Fuel Applications. *Chem. Rev.* **2015**, *115*, 13006−13049.
(43) Peruski, K. M.; Bernales, V.; Dembowski, M.; Lobeck, H. L.; Pellegrini, K. L.; Sigmon, G. E.; Hickam, S.; Wallace, C. M.; Szymanowski, J. E. S.; Balboni, E.; et al. Uranyl Peroxide Cage Cluster Solubility in Water and the Role of the Electrical Double Layer. *Inorg. Chem.* **2017**, *56*, 1333−1339.

https://doi.org/10.1021/acs.chemmater.1c04407
Chem. Mater. 2022, 34, 2771−2778